
Efficient Epistemic Uncertainty Estimation in Regression Ensemble Models Using Pairwise-Distance Estimators

Lucas Berry¹ David Meger¹

Abstract

This work introduces an efficient novel approach for epistemic uncertainty estimation for ensemble models for regression tasks using pairwise-distance estimators (PaiDEs). Utilizing the pairwise-distance between model components, these estimators establish bounds on entropy. We leverage this capability to enhance the performance of Bayesian Active Learning by Disagreement (BALD). Notably, unlike sample-based Monte Carlo estimators, PaiDEs exhibit a remarkable capability to estimate epistemic uncertainty at speeds up to 100 times faster while covering a significantly larger number of inputs at once and demonstrating superior performance in higher dimensions. To validate our approach, we conducted a varied series of regression experiments on commonly used benchmarks: 1D sinusoidal data, *Pendulum*, *Hopper*, *Ant* and *Humanoid*. For each experimental setting, an active learning framework was applied to demonstrate the advantages of PaiDEs for epistemic uncertainty estimation. We compare our approach to existing active learning methods and find that our approach outperforms on high-dimensional regression tasks.

1. Introduction

In this paper, we propose Pairwise-Distance Estimators (PaiDEs) as a non-sample based method for estimating epistemic uncertainty in deep ensembles with probabilistic outputs for regression tasks. Epistemic uncertainty, often distinguished from aleatoric uncertainty, reflects a model’s ignorance and can be reduced by increasing the amount of data available (Hora, 1996; Der Kiureghian & Ditlevsen, 2009; Hüllermeier & Waegeman, 2021). The significance of epistemic uncertainty is particularly pronounced in safety-critical systems, where a single erroneous prediction could

lead to catastrophic consequences (Morales-Torres et al., 2019). Moreover, leveraging epistemic uncertainty proves beneficial as an acquisition criterion for active learning strategies (Houlsby et al., 2011).

Previously Monte Carlo (MC) methods have been employed for estimating epistemic uncertainty, in regression tasks, due to the absence of closed-form expressions in most modeling scenarios (Depeweg et al., 2018; Berry & Meger, 2023). However, as the output dimension increases, these MC methods require a large number of samples to get accurate estimates. PaiDEs offer one non-sample based alternative for estimating information-based criterion in ensemble regression models with probabilistic outputs (Kolchinsky & Tracey, 2017).

Ensembles can be conceptualized as committees, with each ensemble component serving as a committee member (Rokach, 2010). PaiDEs synthesize the consensus amongst a committee of probabilistic learners by calculating the distributional distance between each pair of committee members. Distributional distance is a measure of similarity between two probability distributions. PaiDEs aggregate the pairwise distributional distances in a way that accurately estimates the differential entropy of the entire ensemble. Assuming that the pairwise distances can be efficiently calculated, PaiDEs provide an efficient way to estimate epistemic uncertainty that is not sample-dependent. Figure 1 illustrates a pair of committee members in agreement with low epistemic uncertainty (i.e., small distributional distance) on the right, and another pair in disagreement with high epistemic uncertainty (i.e., large distributional distance) on the left.

This study showcases the application of PaiDEs in estimating epistemic uncertainty on regression tasks for ensembles with probabilistic outputs. Unlike the well-explored area of estimating uncertainty in classification, regression problems pose unique challenges in this field. Information-theoretic quantities such as entropy are more challenging to estimate for an ensemble of continuous distributions compared to an ensemble of categorical distributions, with an ensemble of categorical distributions creating a mixture of categorical distributions which one can easily calculate the entropy for. The primary ensemble utilized in this study is a collection of Normalizing Flows (NFs), known for their effective-

^{*}Equal contribution ¹Department of Computer Science, McGill University, Montreal, Canada. Correspondence to: Lucas Berry <lucas.berry@mail.mcgill.ca>.

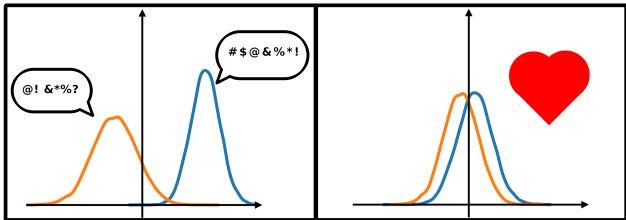


Figure 1: Epistemic uncertainty in an ensemble of probabilistic learners is high when the mixture components disagree (left) and low when there is agreement (right).

ness in capturing heteroscedastic and complex multi-modal aleatoric uncertainty (Rezende & Mohamed, 2015; Kingma & Dhariwal, 2018). This holds particular significance in the realm of robotic locomotion, where these characteristics are pertinent due to the frequent encounters with nonlinear stochastic dynamics. Moreover, these tasks present an ideal application for active learning methods, as acquiring additional data is often resource-intensive and should therefore be conducted with optimal efficiency. Our contributions are as follows:

- We introduce the framework for applying PaiDEs to estimate epistemic uncertainty in deep ensembles with probabilistic outputs (Section 5).
- We extend previous epistemic uncertainty estimation methods to higher dimensional settings, and demonstrate how PaiDEs outperform MC and other active learning benchmarks in the higher dimensional setting with rigorous statistical testing (Section 6).
- We provide an analysis of the time-saving advantages offered by PaiDEs compared to MC estimators for epistemic uncertainty estimation (Section 6.4).

2. Problem Statement

Following a supervised learning framework for regression, let $\mathcal{D} = \{x_i, y_i\}_{i=1}^N$ denote a dataset, where $x_i \in \mathbb{R}^n$ and $y_i \in \mathbb{R}^d$, and our objective is to approximate a complex multi-modal conditional probability $p(y|x)$. Let $f_\theta(y, x)$ denote our approximation to the conditional probability density, where θ is a set of parameters to be learned and is distributed as $p(\theta)$.

Leveraging a learned model, $f_\theta(y, x)$, we wish to estimate uncertainty which is typically viewed from a probabilistic perspective (Cover & Thomas, 2006; Hüllermeier & Waegeman, 2021). When capturing uncertainty in supervised learning, one common measure is that of conditional

differential entropy,

$$H(y|x) = - \int p(y|x) \ln p(y|x) dy.$$

Utilizing conditional differential entropy, we can establish an estimate for epistemic uncertainty as introduced by Hounsby et al. (2011), expressed as:

$$I(y, \theta|x) = H(y|x) - E_{p(\theta)} [H(y|x, \theta)], \quad (1)$$

where $I(\cdot)$ refers to mutual information. Equation 1 demonstrates that epistemic uncertainty, $I(y, \theta|x)$, can be represented by the difference between total uncertainty, $H(y|x)$, and aleatoric uncertainty, $E_{p(\theta)} [H(y|x, \theta)]$. Mutual information measures the information gained about one variable by observing another.

To enable our methods to capture epistemic uncertainty, we employ ensembles to create $p(\theta)$. Ensembles leverage multiple models to obtain the estimated conditional probability by weighting the output distribution from each ensemble component,

$$f_\theta(y, x) = \sum_{j=1}^M \pi_j f_{\theta_j}(y, x) \quad \sum_{j=1}^M \pi_j = 1, \quad (2)$$

where M and $0 \leq \pi_j \leq 1$ are the number of model components and the component weights, respectively. In order to create an ensemble, one of two ways is typically chosen: randomization (Breiman, 2001) or boosting (Freund & Schapire, 1997). While boosting has led to widely used machine learning methods (Chen & Guestrin, 2016), randomization has been the preferred method in deep learning due to its tractability and ease of implementation (Lakshminarayanan et al., 2017).

Utilizing our ensemble we can estimate epistemic uncertainty in decision-making scenarios such as active learning. When all components produce the same $f_{\theta_i}(y, x)$, $I(y, \theta|x)$ is zero, indicating no epistemic uncertainty. Conversely, when the components exhibit varied output distributions, epistemic uncertainty is high. In an active learning framework, one chooses, at each iteration, what data points to add to a training dataset such that the model’s performance improves as much as possible (MacKay, 1992; Settles, 2009). In our context, one chooses the x ’s that maximize Equation 1 and adds those data points to the training set as in Bayesian Active Learning by Disagreement (BALD) (Hounsby et al., 2011). It’s worth noting that in the realm of continuous outputs as in regression and ensemble models, Equation 1 often lacks a closed-form solution, as the entropy of most mixtures of continuous distributions cannot be expressed in closed form (Kolchinsky & Tracey, 2017). Hence, prior methods have resorted to Monte Carlo (MC) estimators for the estimation of epistemic uncertainty (Depeweg et al.,

2018; Postels et al., 2020). One such Monte Carlo method samples K points from the model, $y_j \sim f_\theta(y, x)$, and then estimates the total uncertainty,

$$\hat{H}_{MC}(y|x) = \frac{-1}{K} \sum_{j=1}^K \ln f_\theta(y_j, x).$$

The MC approach approximates the intractable integral over the continuous domain requiring only point-wise evaluation of the ensemble and its components. However, as the number dimensions increases, MC methods typically require a greater number of samples which creates a greater computational burden (Rubinstein & Glynn, 2009).

3. Pairwise-Distance Estimators

Unlike MC methods, PaiDEs completely remove this dependence on sampling by leveraging generalized distance functions between model component distributions. They can be applied when estimating the entropy of mixture distributions as long as the pairwise-distances have a closed-form and thus can be utilized to estimate $H(y|x)$ from Equation 1. The derivation and properties of PaiDEs follow from Kolchinsky & Tracey (2017); we are extending the use of PaiDEs to a supervised learning problem and epistemic uncertainty estimation.

3.1. Properties of Entropy

One can treat a mixture model as a two-step process: first, a component is drawn and, second, a sample is taken from the corresponding component. Let $p(y, \theta|x)$ denote the joint of our output and model components given input x ,

$$p(y, \theta|x) = p(\theta_j|x)p(y|\theta_j, x) = \pi_j p(y|\theta_j, x).$$

Now that we have a representation of the joint, following principles of information theory (Cover & Thomas, 2006), we can write its entropy as,

$$H(y, \theta|x) = H(\theta|y, x) + H(y|x). \quad (3)$$

Additionally, one can show the following bounds for $H(y|x)$,

$$H(y|\theta, x) \leq H(y|x) \leq H(y, \theta|x). \quad (4)$$

Intuitively, the lower bound can be justified by the fact that conditioning on more variables can only decrease or keep entropy the same. The upper bound follows from Equation 3 and $H(\theta|y, x) \geq 0$.

3.2. PaiDEs Definition

Let $D(p_i \parallel p_j)$ denote a generalized distance function between the probability distributions p_i and p_j , which for our

case represent $p_i = p(y|x, \theta_i)$ and $p_j = p(y|x, \theta_j)$, respectively. More specifically, D is referred to as a premetric, $D(p_i \parallel p_j) \geq 0$ and $D(p_i \parallel p_j) = 0$ if $p_i = p_j$. The distance function need not be symmetric nor obey the triangle inequality. As such, PaiDEs can be defined as,

$$\hat{H}_\rho(y|x) := H(y|\theta, x) - \sum_{i=1}^M \pi_i \ln \sum_{j=1}^M \pi_j \exp(-D(p_i \parallel p_j)). \quad (5)$$

PaiDEs have many options for $D(p_i \parallel p_j)$ (Kullback-Leibler divergence, Wasserstein distance, Bhattacharyya distance, Chernoff α -divergence, Hellinger distance, etc.).

Theorem 3.1. *Using the extreme distance functions,*

$$D_{min}(p_i \parallel p_j) = 0 \quad \forall i, j$$

$$D_{max}(p_i \parallel p_j) = \begin{cases} 0, & \text{if } p_i = p_j, \\ \infty, & \text{o/w,} \end{cases}$$

one can show that PaiDEs lie within bounds for entropy established in Equation 4.

Refer to Appendix A for the proof of Theorem 3.1. This provides a general class of estimators but a distance function still needs to be chosen. Certain distance functions improve the bounds in Equation 4.

3.3. Tighter Bounds for PaiDEs

Let the Chernoff α -divergence be defined as (Nielsen, 2011),

$$C_\alpha(p_i \parallel p_j) = -\ln \int p^\alpha(y|x, \theta_i) p^{1-\alpha}(y|x, \theta_j) dy,$$

where $\alpha \in [0, 1]$.

Corollary 3.2. *When applying Chernoff α -divergence as our distance function in Equation 5, we achieve a tighter lower bound than $H(y|\theta, x)$,*

$$\hat{H}_{C_\alpha}(y|x) = H(y|\theta, x) - \sum_{i=1}^M \pi_i \ln \sum_{j=1}^M \pi_j \exp(-C_\alpha(p_i \parallel p_j)), \quad (6)$$

$$H(y|\theta, x) \leq \hat{H}_{C_\alpha}(y|x) \leq H(y|x). \quad (7)$$

Refer to Appendix A for the proof of Corollary 3.2 which follows the steps in Kolchinsky & Tracey (2017). In addition, the tightest lower bound can be shown to be $\alpha = 0.5$ for certain situations (Kolchinsky & Tracey, 2017). Note that when $\alpha = 0.5$, the Chernoff α -divergence is known as the Bhattacharyya distance,

$$D_B(p_i \parallel p_j) = -\ln \int \sqrt{p(y|x, \theta_i)p(y|x, \theta_j)} dy. \quad (8)$$

We utilized PaiDEs with the Bhattacharyya distance, $\hat{H}_{Bhatt}(y|x) = \hat{H}_{C_{0.5}}(y|x)$, as one proposed improvement to MC estimators.

In addition to the improved lower bound, there is an improved upper bound as well. Let Kullback-Liebler (KL) divergence be defined as follows,

$$D_{KL}(p_i \parallel p_j) = \int p(y|x, \theta_i) \ln \frac{p(y|x, \theta_i)}{p(y|x, \theta_j)} dy.$$

Note that the KL divergence does not satisfy the triangle inequality nor is it symmetric, thus it is not metric but does suffice as a generalized distance function.

Corollary 3.3. *When applying Kullback-Liebler divergence as our distance function in Equation 5, we achieve a tighter upper bound than $H(y, \theta|x)$,*

$$\begin{aligned} \hat{H}_{KL}(y|x) &= H(y|\theta, x) \\ &\quad - \sum_{i=1}^M \pi_i \ln \sum_{j=1}^M \pi_j \exp(-D_{KL}(p_i \parallel p_j)), \end{aligned} \quad (9)$$

$$H(y|x) \leq \hat{H}_{KL}(y|x) \leq H(y, \theta|x). \quad (10)$$

Refer to Appendix A for the proof of Corollary 3.3 which follows the steps in Kolchinsky & Tracey (2017). In addition to Bhattacharyya distance, we applied PaiDEs with KL divergence as another proposed improvement to Monte Carlo estimation.

4. Normalizing Flow Ensembles

In this study, we utilize an ensemble technique named Nflows Base, which has previously shown robust performance in estimating both aleatoric and epistemic uncertainty on simulated robotic datasets by leveraging normalizing flows (NFs) to create ensembles (Berry & Meger, 2023). PaiDEs can be employed with any ensemble possessing probabilistic outputs and closed-form distributional distance between ensemble components.

4.1. Nflows Base

NFs have been classically applied to unsupervised tasks (Tabak & Vanden-Eijnden, 2010; Tabak & Turner, 2013; Rezende & Mohamed, 2015), though NFs have been adapted to a supervised learning setting for regression tasks (Winkler et al., 2019; Ardizzone et al., 2019). Using the structure of Winkler et al. (2019), one can define a supervised NF as,

$$\begin{aligned} p_{y|x}(y|x) &= p_{b|x, \theta}(g_\phi^{-1}(y, x)) \\ &\quad \times |\det(J(g_\phi^{-1}(y, x)))|, \\ \log(p_{y|x}(y|x)) &= \log(p_{b|x, \theta}(g_\phi^{-1}(y, x))) \\ &\quad + \log(|\det(J(g_\phi^{-1}(y, x)))|), \end{aligned}$$

where $p_{y|x}$ is the output distribution, $p_{b|x, \theta}$ is the base distribution with parameters θ , J refers to the Jacobian, and $g_\phi^{-1} : y \times x \mapsto b$ is the bijective mapping with parameters ϕ . For a more comprehensive review of NFs, refer to Papamakarios et al. (2021). Nflows Base creates an ensemble in the base distribution,

$$p_{y|x, \theta}(y|x, \theta_j) = p_{b|x, \theta_j}(g_\phi^{-1}(y, x)) |\det(J(g_\phi^{-1}(y, x)))|,$$

where $p_{b|x, \theta}(b|x, \theta_j) = N(\mu_{\theta_j}(x), \Sigma_{\theta_j}(x))$, $\mu_{\theta_j}(x)$ and $\Sigma_{\theta_j}(x)$ denote the mean and covariance for input x and conditioned on θ_j . These parameters are modeled using a neural network with fixed dropout masks to create an ensemble, and diversity is created by randomization and bootstrapping. By constructing the ensemble within the base distribution, one can make use of closed-form pairwise-distance formulae as Berry & Meger (2023) showed that estimating epistemic uncertainty in the base distribution is equivalent to estimating it in the output distribution.

Exploiting these closed-form pairwise-distance formulae, Berry & Meger (2023) showed that Nflows Base outperforms naive NF ensemble methods when estimating epistemic uncertainty. The aleatoric uncertainty from Equation 1 can be estimated in the base distribution space. Therefore aleatoric uncertainty can be computed analytically. This does not apply to the other quantity of Equation 1, total uncertainty, and thus MC techniques were applied in the past to estimate epistemic uncertainty.

5. Epistemic Uncertainty Estimation with PaiDEs

Our extension to prior methodologies empowers the estimation of epistemic uncertainty, the mutual information between y and θ , without the need for sampling. We illustrate this capability for Normalizing Flows (NFs) in the main paper and for probabilistic network ensembles in Figure E (Lakshminarayanan et al., 2017). Note that our proposed estimators can be applied to any ensemble model whose component output distributions have closed-form pairwise-distances. However, given that the space of models with these properties is large, we have decided to focus on Nflows Base for its expressive properties and PNEs as they are widely used (Lakshminarayanan et al., 2017; Chua et al., 2018; Berry & Meger, 2023).

5.1. Epistemic Uncertainty Estimators

By applying our definition of PaiDEs to Equation 1, we obtain the following expression:

$$\begin{aligned} \hat{I}_\rho(y, \theta) &= \hat{H}_\rho(y|x) - E_{p(\theta)} [H(y|x, \theta)] \\ &= - \sum_{i=1}^M \pi_i \ln \sum_{j=1}^M \pi_j \exp(-D(p_i \parallel p_j)), \end{aligned} \quad (11)$$

as $E_{p(\theta)}[H(y|x, \theta)] = H(y|x, \theta)$ leading to cancellation. PaiDEs provide a succinct estimator that can capture epistemic uncertainty with only the pairwise distances between components, thus eliminating reliance on sample-based techniques. We propose the following specific estimators:

$$\hat{I}_{Bhatt}(y, \theta) = - \sum_{i=1}^M \pi_i \ln \sum_{j=1}^M \pi_j \exp(-D_{Bhatt}(p_i \parallel p_j)),$$

$$\hat{I}_{KL}(y, \theta) = - \sum_{i=1}^M \pi_i \ln \sum_{j=1}^M \pi_j \exp(-D_{KL}(p_i \parallel p_j)),$$

where $D_{Bhatt}(p_i \parallel p_j)$ and $D_{KL}(p_i \parallel p_j)$ are defined for Gaussians in Appendix B.

5.2. Combination of PaiDEs & Nflows Base

By combining Nflows Base and PaiDEs, we construct an expressive non-parametric model capable of capturing intricate aleatoric uncertainty in the output distribution while efficiently estimating epistemic uncertainty in the base distribution. Unlike previously proposed methods, we are able to estimate epistemic uncertainty without taking a single sample. Figure 6 in the Appendix shows an example of the distributional pairs that need to be considered in order to estimate epistemic uncertainty for an Nflows Base model.

6. Experimental Results

To evaluate our method, we tested each PaiDE (KL $\hat{I}_{KL}(y, \theta)$ and Bhatt $\hat{I}_{Bhatt}(y, \theta)$) on two 1D environments, as has been previously proposed in the literature (Depeweg et al., 2018). Additionally, we present 4 multi-dimensional environments. In contrast to previous papers (Postels et al., 2020; Ash et al., 2021), we evaluate each method on high dimensional output space (up to 257) to demonstrate the utility of PaiDEs in this setting. Note that, for all experiments, the model components are assumed to be uniform, $\pi_j = \frac{1}{M}$, independent of x . All model hyper-parameters are contained in Appendix B and the code can be found in the supplementary material.

6.1. Data

We evaluated PaiDEs on two 1D benchmarks, *hetero* and *bimodal*. The ground-truth data for *hetero* and *bimodal* can be seen in Figure 2 on the right graphs with the cyan dots. For *hetero*, there are two regions with low density (2 and -2) as can be seen by the green bar chart in the left graph which corresponds to the density of the ground-truth data. In these regions, one would expect a model to have high epistemic uncertainty. For *bimodal*, the number of data points drops off as x increases, thus we would expect a model to have epistemic uncertainty grow as x does. All details for data generation are contained in Appendix C.

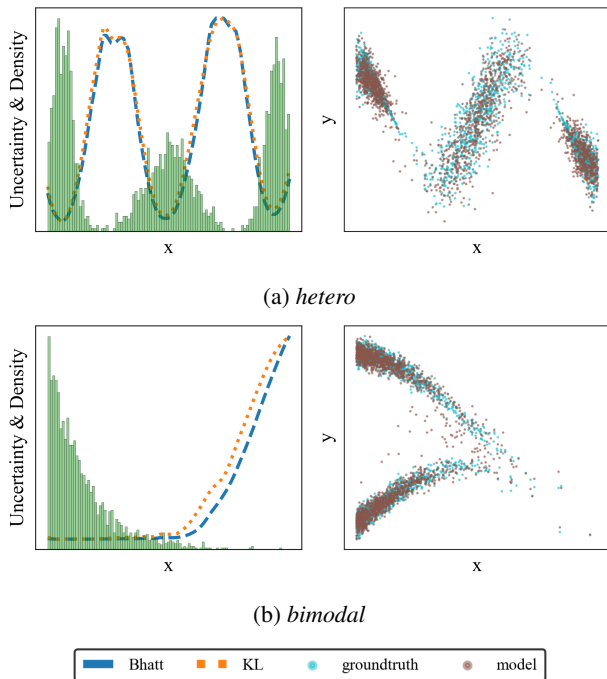


Figure 2: In the right graphs, the brown dots are sampled from Nflows Base and the cyan dots are the ground-truth data. The left graphs depicts the epistemic uncertainty estimates corresponding to our two proposed estimators and the density of the ground-truth data in the green histogram.

In addition to the 1D environments, we tested our methods on four multi-dimensional environments: *Pendulum*, *Hopper*, *Ant*, and *Humanoid* (Todorov et al., 2012). Replay buffers were collected and the dynamics for each environment was modeled, $f_{\theta}(s_t, a_t) = \hat{s}_{t+1}$. The choice of multi-dimensional environments is motivated by their common use as benchmarks and their higher-dimensional output space, providing a robust validation of our methods. Note that, for *Ant* and *Humanoid*, the dimensions representing their contact forces were eliminated due to a bug in Mujoco-v2¹.

6.2. 1D Experiments

Our 1D environments provide empirical proof that PaiDEs can accurately measure epistemic uncertainty. Figure 2 depicts that both KL and Bhatt are proficient at estimating the epistemic uncertainty as each method shows an increase in epistemic uncertainty around 2 and -2 on the *hetero* setting. This can be seen from the blue and orange lines with both estimators performing similarly.

A similar pattern can be seen for the *bimodal* setting in Figure 2, which shows that both Bhatt and KL can accurately

¹More information can be found here: <https://github.com/openai/gym/issues/1541>.

Table 1: Mean RMSE on the test set for the last (100^{th}) Acquisition Batch for Nflows Base. Experiments were across ten different seeds and the results are expressed as mean \pm standard deviation. The best means are in bold and results that are statistically significant are highlighted.

	<i>hetero</i>	<i>bimodal</i>	<i>Pendulum</i>	<i>Hopper</i>	<i>Ant</i>	<i>Humanoid</i>
Output Dim.	1	1	3	11	32	257
Random	1.56 ± 0.14	6.4 ± 0.62	0.15 ± 0.04	0.97 ± 0.2	1.05 ± 0.1	6.59 ± 1.54
BatchBALD	6.62 ± 1.84	6.07 ± 0.12	0.06 ± 0.03	0.62 ± 0.18	1.93 ± 0.3	11.28 ± 0.16
BADGE	6.03 ± 1.68	6.25 ± 0.33	0.07 ± 0.04	0.62 ± 0.21	2.11 ± 0.26	10.99 ± 0.33
BAIT	7.39 ± 0.58	6.2 ± 0.41	0.08 ± 0.05	0.68 ± 0.23	1.91 ± 0.22	11.01 ± 0.23
LCMD	5.69 ± 1.03	6.24 ± 0.34	0.06 ± 0.03	0.64 ± 0.2	1.84 ± 0.17	11.35 ± 0.16
MC	1.54 ± 0.17	6.01 ± 0.04	0.06 ± 0.01	0.32 ± 0.02	1.01 ± 0.05	10.71 ± 0.43
KL	1.47 ± 0.15	6.01 ± 0.04	0.05 ± 0.04	0.3 ± 0.03	1.06 ± 0.08	3.4 ± 0.48
Bhatt	1.55 ± 0.31	6.0 ± 0.04	0.05 ± 0.01	0.29 ± 0.03	1.1 ± 0.07	3.37 ± 0.44

■ $p < 0.05$
■ $p < 0.01$
■ $p < 0.001$

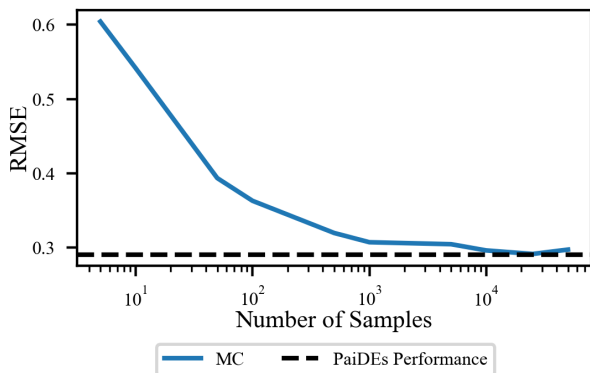


Figure 3: RMSE on the test set at the 100^{th} acquisition batch of the MC estimator on the *Hopper* environment as the number of samples, K , per input, x , increases. Experiment were run across 10 seeds and the mean is being reported.

capture epistemic uncertainty. Each estimator shows the pattern of increasing epistemic uncertainty where the data is more scarce. Both examples show accurate epistemic uncertainty estimation with no loss in aleatoric uncertainty representation, as demonstrated in the right graphs in Figure 2: the brown dots closely match the cyan dots. Note that for visual clarity, the epistemic uncertainty has been scaled to 0-1, while ensuring that the relative properties of the estimators are preserved. Further discussion on over- and underestimation is provided in Appendix D.

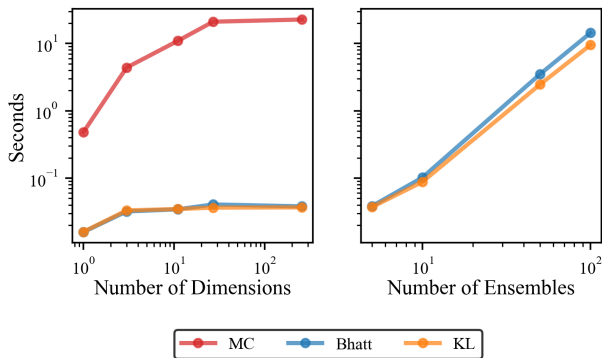


Figure 4: On the left, the amount of time taken for each estimator across the different settings (1, 3, 11, 27, 257 dimensions). On the right, the amount of time taken for PaiDEs as the number of ensemble components increases for the 257 dimensional setting. Results are averaged over 10 seeds and shown on a log scale.

6.3. Active Learning

While the 1D experiments provide evidence of PaiDEs’ effectiveness for estimating epistemic uncertainty, the active learning experiments extend this evaluation to higher-dimensional data and for a decision-making task. In order to benchmark our method, we compare against four state-of-the-art active learning frameworks: BatchBALD (Kirsch et al., 2019), BADGE (Ash et al., 2019), BAIT (Ash et al., 2021) and LCMD (Holzmüller et al., 2023). Additionally, a random baseline is included. The training set is initialized

with 100 or 200 data points for 1D and multi-dimensional environments, respectively. In each acquisition batch, 10 points are added. For the Monte Carlo (MC) estimator, 1,000 unseen inputs were sampled, and their epistemic uncertainties estimated, except for the *Humanoid* environment where only 100 new inputs were sampled due to computational constraints. In contrast, PaiDEs sampled 10,000 new inputs and estimated their epistemic uncertainties for each environment including *Humanoid*. This underscores one advantage of PaiDEs over MC estimators, as they can estimate epistemic uncertainty over larger regions at a lower computational cost than their MC counterparts. Note that the other benchmarks each sampled 10,000 inputs as well and their respective acquisition functions applied. The root mean squared error (RMSE) on the test set was calculated at each acquisition batch to evaluate performance.

Table 1 displays the performance of each framework on the 100th acquisition batch. In each environment, we conducted a Welch’s t-test that compares both PaiDE estimators against each baseline. We included a Holm–Bonferroni correction to control the family-wise error rate, for more information refer to Appendix G. For each data setting, the PaiDEs reach lower or comparable RMSEs compared to each benchmark, demonstrating their efficacy in estimating epistemic uncertainty. Notably, in higher dimensions, PaiDEs outperform other methods in a statistically significant manner, as are shown in the *Humanoid*. The learning curves can be seen in Figure 5.

To conduct a more in-depth analysis of our proposed method, we compared PaiDEs to MC estimators with a varying sample size, K , in the *Hopper* environment. We expected that MC estimators would perform on par with PaiDEs with a sufficient number of samples. This trend is illustrated in Figure 3. The MC estimator does reach the peak performance of PaiDEs given enough samples but does not perform better than PaiDEs, suggesting that PaiDEs are sufficient when estimating epistemic uncertainty in this context.

6.4. Time Analysis & Limitations

In addition to benchmarking PaiDEs on active learning experiments, we provide an analysis of the time gains across our experiments. The left hand side of Figure 4 depicts the speed increase that can be gained using PaiDEs over an MC approach. A 1-2 order magnitude of improvement can be seen. The estimates are obtained from the active learning experiments, and the number of dimensions correspond to each of the environments.

A weakness of PaiDEs is that, as the number of components increases, the computational cost rises due to its quadratic complexity. In the instance where the distance is not symmetric, KL-divergence, $M^2 - M$ pairwise-distances need to be computed. For symmetric distances, such as Bhat-

tacharyaa distance, only $\frac{M^2 - M}{2}$ distances need to be computed. The right hand side of Figure 4 shows an analysis of the time taken as the number of ensembles grow. Note that for Bhatt, the time costs could be improved upon using the symmetry logic described, the results shown calculated all pairwise-distances. Despite the growing complexity of PaiDEs with the number of components, this is normally not a problem for deep learning ensembles as they have a relatively low number (5-10) of components (Osband et al., 2016; Chua et al., 2018).

An additional limitation is the bias introduced by PaiDEs, which MC estimators do not suffer from. It is essential to note that, in the context of active learning, epistemic uncertainty serves as a relative quantity for comparing potential acquisition points. The introduction of bias from PaiDEs does not impact the relative relationship of epistemic uncertainty between different data points in our experiments. We demonstrate that the relative relationship of epistemic uncertainty remains intact in Appendix D.

7. Related Work

Researchers have employed Bayesian neural networks alongside information-based criteria for active learning in image classification problems (Gal et al., 2017; Kendall & Gal, 2017; Kirsch et al., 2019). In addition to these methods, others have proposed frameworks that utilize gradient embeddings in lieu of information-based criterion (Ash et al., 2019; 2021; Holzmüller et al., 2023). While the majority of these methods focus on image classification, a few methods have applications in regression (Ash et al., 2021; Holzmüller et al., 2023). In these cases, both Ash et al. (2021) and Holzmüller et al. (2023) only address 1D regression problems. In contrast, our research focuses on active learning in high-dimensional output space, up to 257 dimensions. In doing so, we address a gap in the literature which has importance in such fields as robotic locomotion, where gathering new data comes at high costs.

In addition to Bayesian methods, ensembles have been harnessed for epistemic uncertainty estimation (Lakshminarayanan et al., 2017; Choi et al., 2018; Chua et al., 2018). Specifically related to our work, ensembles have been leveraged to quantify epistemic uncertainty in regression problems and active learning (Depeweg et al., 2018; Postels et al., 2020; Berry & Meger, 2023). Depeweg et al. (2018) employed Bayesian neural networks to model mixtures of Gaussians and demonstrated their ability to measure uncertainty in low-dimensional environments (1-2D). Building upon this foundation, Postels et al. (2020) and Berry & Meger (2023) extended the research by developing efficient Normalizing Flow (NF) ensemble models that effectively captured epistemic uncertainty. Our work advances this line of research by eliminating the need for sampling to esti-

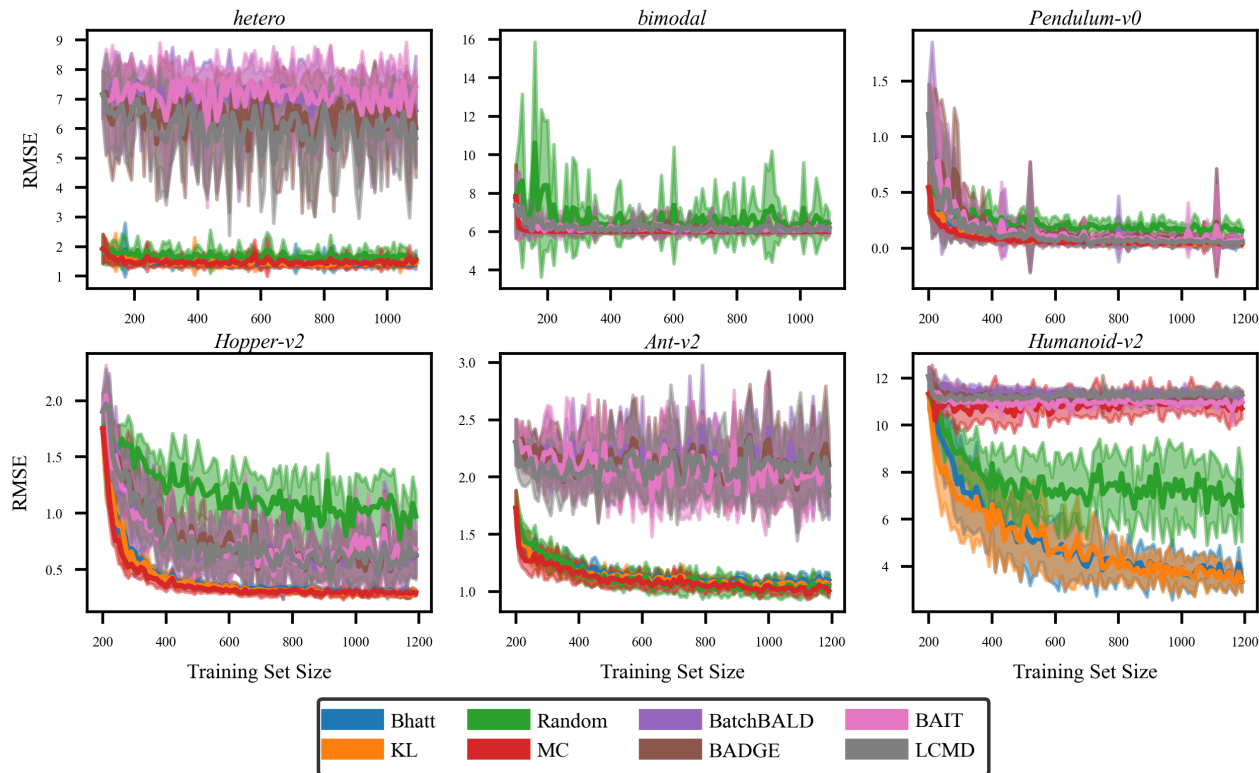


Figure 5: Mean RMSE on the test set as data was added to the training set for Nflows Base.

mate epistemic uncertainty, resulting in a faster and more effective method, especially in higher dimensions.

Entropy estimators, which do not rely on sampling, is an active area of research (Jebara & Kondor, 2003; Jebara et al., 2004; Huber et al., 2008; Kolchinsky & Tracey, 2017). Kulak et al. (2021) and Kulak & Calinon (2021) demonstrated the utility of Pairwise-Distance Estimators (PaiDEs) within Bayesian contexts, employing PaiDEs to estimate conditional predictive posterior entropy. In contrast, our approach provides a more general estimate of epistemic uncertainty, as defined in Equation 1, which can be applied to both ensemble and Bayesian methods. Furthermore, our method is adaptable to flexible deep learning models, a capability that was previously unavailable in the approach presented by Kulak et al. (2021) and Kulak & Calinon (2021).

Several methods have emerged in the literature for estimating epistemic uncertainty without relying on sampling techniques (Van Amersfoort et al., 2020; Charpentier et al., 2020). Both Van Amersfoort et al. (2020) and Charpentier et al. (2020) focus on classification tasks with 1D categorical outputs. Charpentier et al. (2021) extends the work of Charpentier et al. (2020) to regression tasks but is limited to modeling outputs as members of the exponential family.

In contrast, our approach can handle more complex output distributions by directly considering the outputs from Normalizing Flows (NFs) and can be applied to a larger space of regression models. This flexibility is particularly valuable in scenarios involving intricate non-linear robotic dynamics, as demonstrated in our experiments.

8. Conclusions

In this study, we introduced two epistemic uncertainty estimators and applied them to expressive ensemble models. We depicted how our method can be used to more efficiently quantify uncertainty by leveraging closed-form pairwise-distance instead of sampling. This led to improvements in computational speed and accuracy, especially in larger dimensions. As learning becomes pervasive in high-dimensional and complex tasks in society, our method is well-placed to enable epistemic uncertainty awareness without undue computing overhead.

Impact Statement

This paper presents work whose goal is to advance the field of Machine Learning. There are many potential societal

consequences of our work, none which we feel must be specifically highlighted here.

References

- Ardizzone, L., Lüth, C., Kruse, J., Rother, C., and Köthe, U. Guided image generation with conditional invertible neural networks. *arXiv preprint arXiv:1907.02392*, 2019.
- Ash, J., Goel, S., Krishnamurthy, A., and Kakade, S. Gone fishing: Neural active learning with fisher embeddings. *Advances in Neural Information Processing Systems*, 34: 8927–8939, 2021.
- Ash, J. T., Zhang, C., Krishnamurthy, A., Langford, J., and Agarwal, A. Deep batch active learning by diverse, uncertain gradient lower bounds. In *International Conference on Learning Representations*, 2019.
- Berry, L. and Meger, D. Normalizing flow ensembles for rich aleatoric and epistemic uncertainty modeling. *Proceedings of the AAAI Conference on Artificial Intelligence*, 37(6):6806–6814, 2023.
- Breiman, L. Random forests. *Machine learning*, 45(1): 5–32, 2001.
- Brockman, G., Cheung, V., Pettersson, L., Schneider, J., Schulman, J., Tang, J., and Zaremba, W. Openai gym. *arXiv preprint arXiv:1606.01540*, 2016.
- Charpentier, B., Zügner, D., and Günnemann, S. Posterior network: Uncertainty estimation without ood samples via density-based pseudo-counts. *Advances in Neural Information Processing Systems*, 33:1356–1367, 2020.
- Charpentier, B., Borchert, O., Zügner, D., Geisler, S., and Günnemann, S. Natural posterior network: Deep bayesian uncertainty for exponential family distributions. *arXiv preprint arXiv:2105.04471*, 2021.
- Chen, T. and Guestrin, C. Xgboost: A scalable tree boosting system. In *Proceedings of the 22nd acm sigkdd international conference on knowledge discovery and data mining*, pp. 785–794, 2016.
- Choi, H., Jang, E., and Alemi, A. A. Waic, but why? generative ensembles for robust anomaly detection. *arXiv preprint arXiv:1810.01392*, 2018.
- Chua, K., Calandra, R., McAllister, R., and Levine, S. Deep reinforcement learning in a handful of trials using probabilistic dynamics models. In *Advances in Neural Information Processing Systems*, volume 31, 2018.
- Colas, C., Sigaud, O., and Oudeyer, P.-Y. A hitchhiker’s guide to statistical comparisons of reinforcement learning algorithms. *arXiv preprint arXiv:1904.06979*, 2019.
- Cover, T. M. and Thomas, J. A. *Elements of information theory*. Wiley-Interscience, 2006.
- Depeweg, S., Hernandez-Lobato, J.-M., Doshi-Velez, F., and Udluft, S. Decomposition of uncertainty in bayesian deep learning for efficient and risk-sensitive learning. In *International Conference on Machine Learning*, pp. 1184–1193. PMLR, 2018.
- Der Kiureghian, A. and Ditlevsen, O. Aleatory or epistemic? does it matter? *Structural safety*, 31(2):105–112, 2009.
- Durkan, C., Bekasov, A., Murray, I., and Papamakarios, G. Cubic-spline flows. In *Workshop on Invertible Neural Networks and Normalizing Flows, International Conference on Machine Learning*, 2019.
- Durkan, C., Bekasov, A., Murray, I., and Papamakarios, G. nflows: normalizing flows in PyTorch. <https://doi.org/10.5281/zenodo.4296287>, Nov 2020. Accessed: 2021-09-01.
- Freund, Y. and Schapire, R. E. A decision-theoretic generalization of on-line learning and an application to boosting. *Journal of computer and system sciences*, 55(1):119–139, 1997.
- Gal, Y., Islam, R., and Ghahramani, Z. Deep bayesian active learning with image data. In *International Conference on Machine Learning*, pp. 1183–1192. PMLR, 2017.
- Harakeh, A. and Waslander, S. L. Estimating and evaluating regression predictive uncertainty in deep object detectors. *arXiv preprint arXiv:2101.05036*, 2021.
- Haussler, D. and Opper, M. Mutual information, metric entropy and cumulative relative entropy risk. *The Annals of Statistics*, 25(6):2451–2492, 1997.
- Hershey, J. R. and Olsen, P. A. Approximating the kullback leibler divergence between gaussian mixture models. In *2007 IEEE International Conference on Acoustics, Speech and Signal Processing-ICASSP’07*, volume 4, pp. IV–317. IEEE, 2007.
- Holzmüller, D., Zaverkin, V., Kästner, J., and Steinwart, I. A framework and benchmark for deep batch active learning for regression. *Journal of Machine Learning Research*, 24(164):1–81, 2023.
- Hora, S. C. Aleatory and epistemic uncertainty in probability elicitation with an example from hazardous waste management. *Reliability Engineering & System Safety*, 54(2-3):217–223, 1996.
- Houlsby, N., Huszár, F., Ghahramani, Z., and Lengyel, M. Bayesian active learning for classification and preference learning. *arXiv preprint arXiv:1112.5745*, 2011.

- Huber, M. F., Bailey, T., Durrant-Whyte, H., and Hanebeck, U. D. On entropy approximation for gaussian mixture random vectors. In *2008 IEEE International Conference on Multisensor Fusion and Integration for Intelligent Systems*, pp. 181–188. IEEE, 2008.
- Hüllermeier, E. and Waegeman, W. Aleatoric and epistemic uncertainty in machine learning: An introduction to concepts and methods. *Machine Learning*, 110(3):457–506, 2021.
- Jebara, T. and Kondor, R. Bhattacharyya and expected likelihood kernels. In *Learning theory and kernel machines*, pp. 57–71. Springer, 2003.
- Jebara, T., Kondor, R., and Howard, A. Probability product kernels. *The Journal of Machine Learning Research*, 5: 819–844, 2004.
- Kendall, A. and Gal, Y. What uncertainties do we need in bayesian deep learning for computer vision? *Advances in neural information processing systems*, 30, 2017.
- Kingma, D. P. and Dhariwal, P. Glow: Generative flow with invertible 1x1 convolutions. *Advances in neural information processing systems*, 31, 2018.
- Kirsch, A. Black-box batch active learning for regression. *arXiv preprint arXiv:2302.08981*, 2023.
- Kirsch, A., Van Amersfoort, J., and Gal, Y. Batchbald: Efficient and diverse batch acquisition for deep bayesian active learning. *Advances in neural information processing systems*, 32, 2019.
- Kolchinsky, A. and Tracey, B. D. Estimating mixture entropy with pairwise distances. *Entropy*, 19(7):361, 2017.
- Kulak, T. and Calinon, S. Combining social and intrinsically-motivated learning for multi-task robot skill acquisition. *IEEE Transactions on Cognitive and Developmental Systems*, 2021.
- Kulak, T., Girgin, H., Odobez, J.-M., and Calinon, S. Active learning of bayesian probabilistic movement primitives. *IEEE Robotics and Automation Letters*, 6(2):2163–2170, 2021.
- Kurutach, T., Clavera, I., Duan, Y., Tamar, A., and Abbeel, P. Model-ensemble trust-region policy optimization. *arXiv preprint arXiv:1802.10592*, 2018.
- Lakshminarayanan, B., Pritzel, A., and Blundell, C. Simple and scalable predictive uncertainty estimation using deep ensembles. *Advances in neural information processing systems*, 30, 2017.
- MacKay, D. J. Information-based objective functions for active data selection. *Neural computation*, 4(4):590–604, 1992.
- Morales-Torres, A., Escuder-Bueno, I., Serrano-Lombillo, A., and Rodríguez, J. T. C. Dealing with epistemic uncertainty in risk-informed decision making for dam safety management. *Reliability Engineering & System Safety*, 191:106562, 2019.
- Nielsen, F. Chernoff information of exponential families. *arXiv preprint arXiv:1102.2684*, 2011.
- Osband, I., Blundell, C., Pritzel, A., and Van Roy, B. Deep exploration via bootstrapped dqn. *Advances in neural information processing systems*, 29, 2016.
- Paisley, J. W. Two useful bounds for variational inference. 2010. URL <https://api.semanticscholar.org/CorpusID:15745903>.
- Papamakarios, G., Nalisnick, E. T., Rezende, D. J., Mohamed, S., and Lakshminarayanan, B. Normalizing flows for probabilistic modeling and inference. *J. Mach. Learn. Res.*, 22(57):1–64, 2021.
- Postels, J., Blum, H., Strümler, Y., Cadena, C., Siegwart, R., Van Gool, L., and Tombari, F. The hidden uncertainty in a neural networks activations. *arXiv preprint arXiv:2012.03082*, 2020.
- Rezende, D. and Mohamed, S. Variational inference with normalizing flows. In *Proceedings of the 32nd International Conference on Machine Learning*, volume 37 of *Proceedings of Machine Learning Research*, pp. 1530–1538, Lille, France, 07–09 Jul 2015.
- Rokach, L. *Pattern classification using ensemble methods*, volume 75. World Scientific, 2010.
- Rubinstein, R. Y. and Glynn, P. W. How to deal with the curse of dimensionality of likelihood ratios in monte carlo simulation. *Stochastic Models*, 25(4):547–568, 2009.
- Settles, B. Active learning literature survey. *Synthesis Lectures on Artificial Intelligence and Machine Learning*, 2009.
- Tabak, E. G. and Turner, C. V. A family of nonparametric density estimation algorithms. *Communications on Pure and Applied Mathematics*, 66(2):145–164, 2013.
- Tabak, E. G. and Vanden-Eijnden, E. Density estimation by dual ascent of the log-likelihood. *Communications in Mathematical Sciences*, 8(1):217–233, 2010.
- Todorov, E., Erez, T., and Tassa, Y. Mujoco: A physics engine for model-based control. In *2012 IEEE/RSJ international conference on intelligent robots and systems*, pp. 5026–5033. IEEE, 2012.

Van Amersfoort, J., Smith, L., Teh, Y. W., and Gal, Y. Uncertainty estimation using a single deep deterministic neural network. In *International conference on machine learning*, pp. 9690–9700. PMLR, 2020.

Winkler, C., Worrall, D., Hoozeboom, E., and Welling, M. Learning likelihoods with conditional normalizing flows. *arXiv preprint arXiv:1912.00042*, 2019.

A. Proofs

The proofs follow from the steps of [Kolchinsky & Tracey \(2017\)](#).

Proof of Theorem 3.1

Proof. Applying $D_{min}(p_i \parallel p_j)$ as our distance in PaiDEs,

$$\begin{aligned} \hat{H}(Y|X) &= H(Y|X, \Theta) - \sum_{i=1}^M \pi_i \ln \sum_{j=1}^M \pi_j \exp(-D_{min}(p_i \parallel p_j)) \\ &= H(Y|X, \Theta) - \sum_{i=1}^M \pi_i \ln \sum_{j=1}^M \pi_j \\ &= H(Y|X, \Theta). \end{aligned}$$

Note the last line follows from the fact that the component weights must sum to one, $\sum_{j=1}^M \pi_j = 1$. Next using $D_{max}(p_i \parallel p_j)$,

$$\begin{aligned} \hat{H}(Y|X) &= H(Y|X, \Theta) - \sum_{i=1}^M \pi_i \ln \sum_{j=1}^M \pi_j \exp(-D_{max}(p_i \parallel p_j)) \\ &= H(Y|X, \Theta) - \sum_{i=1}^M \pi_i \ln \left(\pi_i + \sum_{j \neq i} \pi_j \exp(-D_{max}(p_i \parallel p_j)) \right) \\ &= H(Y|X, \Theta) - \sum_{i=1}^M \pi_i \ln \pi_i \\ &= H(Y|X, \Theta) + H(\Theta|X) \\ &= H(Y, \Theta|X). \end{aligned}$$

This shows the upper bound with $D_{max}(p_i \parallel p_j)$ and the lower bound with $D_{min}(p_i \parallel p_j)$. Note that in our case $H(\Theta|X) = H(\Theta)$ as the distribution of weights does not depend on our input. \square

Proof of Corollary 3.2

Proof. To show the upper bound from [Equation 7](#) we use a derivation from [Haussler & Opper \(1997\)](#),

$$\begin{aligned} H(Y|X) &= H(Y|X, \Theta) - \int \sum_{i=1}^M \pi_i p_i(y|x) \ln \frac{p_{Y|X}(y|x)}{p_i(y|x)} dy \\ &= H(Y|X, \Theta) - \int \sum_{i=1}^M \pi_i p_i(y|x) \ln \frac{p_{Y|X}(y|x)}{p_i(y|x)^{1-\alpha} \sum_j \pi_j p_j(y|x)^{1-\alpha}} dy \\ &\quad - \int \sum_{i=1}^M \pi_i p_i(y|x) \ln \frac{\sum_j \pi_j p_j(y|x)^{1-\alpha}}{p_i(y|x)^\alpha} dy \\ &\geq H(Y|X, \Theta) - \int \sum_{i=1}^M \pi_i p_i(y|x) \ln \frac{\sum_j \pi_j p_j(y|x)^{1-\alpha}}{p_i(y|x)^\alpha} dy \\ &\geq H(Y|X, \Theta) - \sum_{i=1}^M \pi_i \ln \int p_i(y|x)^\alpha \sum_j \pi_j p_j(y|x)^{1-\alpha} dy \\ &= H(Y|X, \Theta) - \sum_{i=1}^M \pi_i \ln \sum_{j=1}^M \pi_j \exp(-C_\alpha(p_i \parallel p_j)). \end{aligned}$$

The two inequalities follow from Jensen's inequality. \square

Proof of Corollary 3.3

Proof. The lower bound can be shown using the definition of entropy for a mixture,

$$\begin{aligned}
 H(Y|X) &= - \sum_{i=1}^M \pi_i E \left[\ln \sum_{j=1}^M \pi_j p_j(y|x) \right] \\
 &\leq - \sum_{i=1}^M \pi_i \ln \sum_{j=1}^M \pi_j \exp(E_{p_i}[\ln p_j(y|x)]) \\
 &= - \sum_{i=1}^M \pi_i \ln \sum_{j=1}^M \pi_j \exp(-H(p_i \| p_j)) \\
 &= \sum_{i=1}^M \pi_i H(p_i) - \sum_{i=1}^M \pi_i \ln \sum_{j=1}^M \pi_j \exp(-KL(p_i \| p_j)) \\
 &= H(Y|X, \Theta) - \sum_{i=1}^M \pi_i \ln \sum_{j=1}^M \pi_j \exp(-KL(p_i \| p_j)),
 \end{aligned}$$

where E_{p_i} refers to the expectation when Y is distributed as p_i and $H(p_i \| p_j)$ indicates the cross entropy. The inequality in line 2 follows from [Hershey & Olsen \(2007\)](#) and [Paisley \(2010\)](#). \square

B. Compute and Hyper-parameter Details

The Nflows Base model employed one nonlinear transformation, g , with a single hidden layer containing 20 units, utilizing cubic spline flows as per ([Durkan et al., 2019](#)). The base network consisted of two hidden layers, each comprising 40 units with ReLU activation functions. It is important to note that all base distributions were Gaussian. The PNEs adopted an architecture of three hidden layers each with 50 units and ReLU activation functions. Model hyperparameters remained consistent across all experiments. Training was conducted using 16GB RAM on Intel Gold 6148 Skylake @ 2.4 GHz CPUs and NVidia V100SXM2 (16G memory) GPUs. For each experimental setting, PNEs and Nflows Base were executed with five ensemble components. The MC estimator sampled 1000 and 5000 points for Nflows Base and PNEs, respectively, for each x conditioned on. The nflows library ([Durkan et al., 2020](#)) and the BMDAL library ([Kirsch, 2023](#)) were employed with minor modifications.

Note that for the Bhatt estimator, the Bhattacharyya distance between two Gaussians is,

$$\begin{aligned}
 D_B(p_i \| p_j) &= \frac{1}{8} (\mu_{i|x} - \mu_{j|x})^T \Sigma^{-1} (\mu_{i|x} - \mu_{j|x}) + \frac{1}{2} \ln \left(\frac{\det \Sigma}{\sqrt{\det \Sigma_{i|x} \det \Sigma_{j|x}}} \right), \\
 \Sigma &= \frac{\Sigma_{i|x} + \Sigma_{j|x}}{2}.
 \end{aligned}$$

Also note that for the KL estimator, the KL divergence between two Gaussians is,

$$D_{KL}(p_i \| p_j) = \frac{1}{2} \left(\text{tr}(\Sigma_{j|x}^{-1} \Sigma_{i|x}) - D + \ln \left(\frac{\det \Sigma_{j|x}}{\det \Sigma_{i|x}} \right) + (\mu_{j|x} - \mu_{i|x})^T \Sigma_{j|x}^{-1} (\mu_{j|x} - \mu_{i|x}) \right),$$

where $\text{tr}(\cdot)$ refers to the trace of a matrix.

C. Data

The *hetero* dataset was generated using a two step process. Firstly, a categorical distribution with three values was sampled, where $p_i = \frac{1}{3}$. Secondly, x was drawn from one of three different Gaussian distributions ($N(-4, \frac{2}{5})$, $N(0, \frac{9}{10})$, $N(4, \frac{2}{5})$)

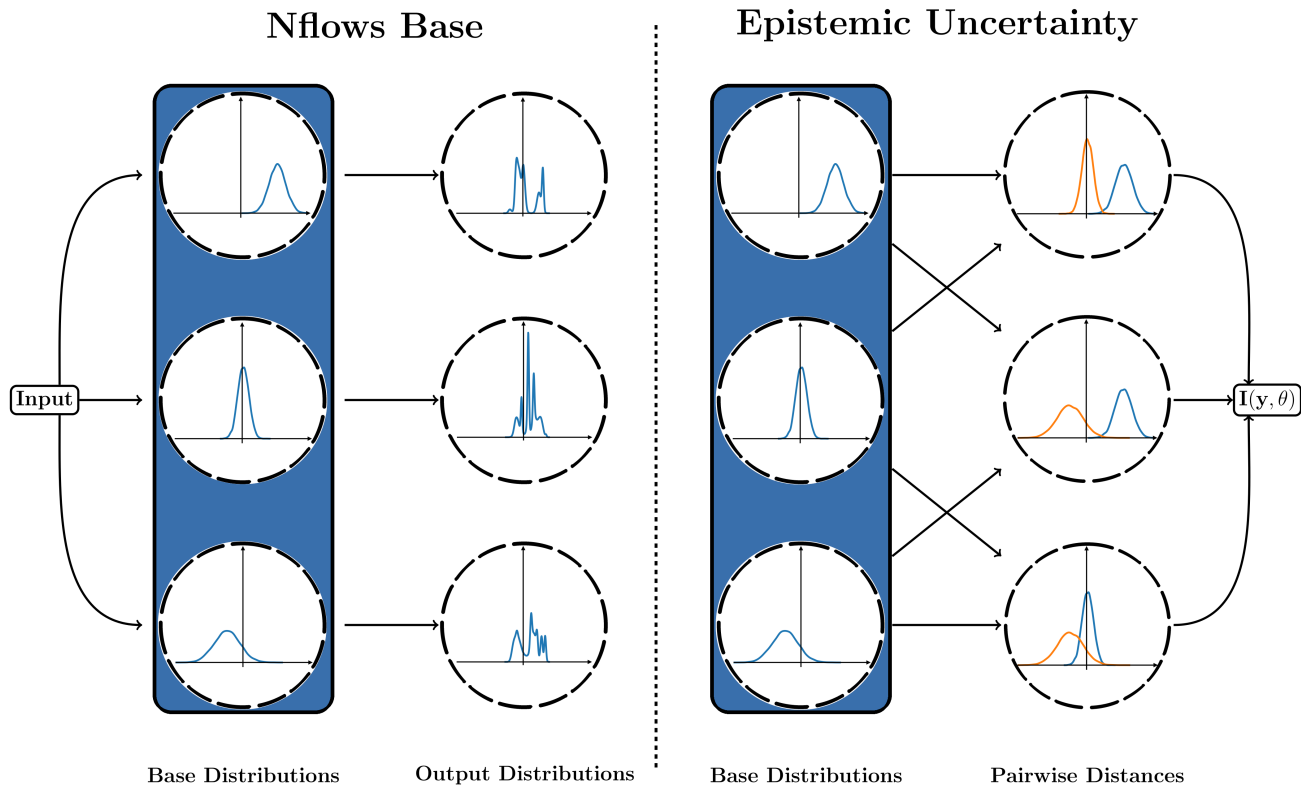


Figure 6: Nflows Base as an ensemble of 3 components with one bijective transformation on the left and an example of the pairwise comparisons needed to estimate epistemic uncertainty for said model on the right. Note the base distributions, instead of the output distributions, from Nflows Base are used to estimate the epistemic uncertainty which are highlighted by the blue bar.

based on the value of the categorical distribution. The corresponding y was then generated as follows:

$$y = 7 \sin(x) + 3z \left| \cos\left(\frac{x}{2}\right) \right|.$$

On the other hand, the *bimodal* dataset was created by sampling x from an exponential distribution with parameter $\lambda = 2$, and then sampling n from a Bernoulli distribution with $p = 0.5$. Based on the value of n , the y value was determined as:

$$y = \begin{cases} 10 \sin(x) + z & n = 0 \\ 10 \cos(x) + z + 20 - x & n = 1 \end{cases}.$$

Note that for both *bimodal* and *hetero* data $z \sim N(0, 1)$.

Regarding the multi-dimensional environments, namely *Pendulum*, *Hopper*, *Ant*, and *Humanoid*, the training sets and test sets were collected using different approaches. The training sets were obtained by applying a random policy, while the test sets were generated using an expert policy. This methodology was employed to ensure diversity between the training and test datasets. Notably, the OpenAI Gym library was utilized, with minor modifications (Brockman et al., 2016).

D. Additional Results

We provide an analysis of the bias introduced by PaiDEs in Figure 7. Note that in Figure 2 the epistemic uncertainty values mapped to 0-1 via a min-max normalization. Both plots show that PaiDEs introduce some bias in the 1D settings, though this is not a problem in an active learning setting as we only care about a point’s uncertainty relative to other points and this relationship is preserved. In addition to Table 1, we provide Figure 5 to show the entire active learning curve and Table 2 detailing more acquisition batches. The pattern of PaiDEs outperforming or perform similarly to baselines holds across all environments and acquisition batches. An additional metric we evaluated on was log-likelihood, as the log-likelihood has been shown to be a proper scoring rule (Harakeh & Waslander, 2021). The results are shown in Figure 8, with 10 seeds being run and mean standard deviation being reported. As can be seen, the KL and Bhatt estimators perform similarly or better than the MC estimator on all environments. Note that due to the high-dimensional setting of *Humanoid* the log-likelihood for each estimator did not improve as data was added. This is due to the fact, that in order to calculate the log-likelihood of the ensemble one needs to calculate the likelihood of each individual model and then sum them together. In this process we are more likely to run into an issue of values being rounded to zero as we cannot store enough digits. As in Table 1, we have recorded certain acquisition batches in Table 3. Lastly, we provide a comparison on *Hopper* of the MC estimator to PaiDEs as the number samples drawn is increased in Figure 9.

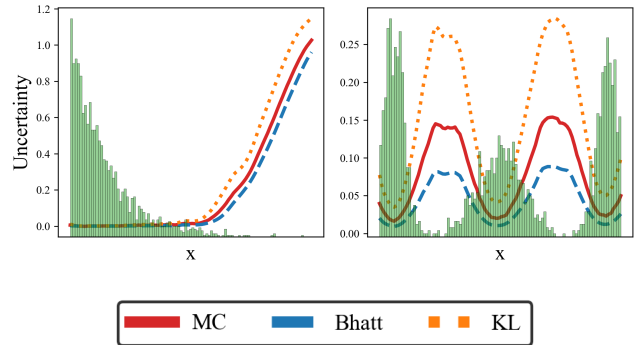


Figure 7: The bias introduced by PaiDEs for Nflows Base compared to the MC method on the 1D environments.

Efficient Epistemic Uncertainty Estimation

Table 2: Mean RMSE on the test set for certain Acquisition Batches for Nflows Base. Experiments were across ten different seeds and the results are expressed as mean plus minus one standard deviation.

Env	Acq. Batch	Random	BatchBALD	BADGE	BAIT	LCMD	Monte Carlo	KL	Bhatt
<i>hetero</i>	10	1.76 ± 0.17	6.81 ± 1.74	6.31 ± 2.05	6.89 ± 1.64	6.51 ± 1.22	1.48 ± 0.2	1.66 ± 0.2	1.56 ± 0.26
	25	1.69 ± 0.45	6.98 ± 1.48	7.14 ± 0.72	7.64 ± 0.6	6.77 ± 0.75	1.44 ± 0.1	1.42 ± 0.12	1.42 ± 0.11
	50	1.64 ± 0.22	7.26 ± 0.63	6.58 ± 0.91	7.46 ± 0.61	6.16 ± 0.88	1.45 ± 0.12	1.49 ± 0.29	1.42 ± 0.11
	100	1.56 ± 0.14	6.62 ± 1.84	6.03 ± 1.68	7.39 ± 0.58	5.69 ± 1.03	1.54 ± 0.17	1.47 ± 0.15	1.55 ± 0.31
<i>bimodal</i>	10	8.4 ± 3.38	6.07 ± 0.13	6.07 ± 0.09	6.03 ± 0.05	6.19 ± 0.18	6.02 ± 0.05	6.01 ± 0.05	6.01 ± 0.05
	25	6.1 ± 0.08	6.07 ± 0.09	6.17 ± 0.21	6.19 ± 0.23	6.14 ± 0.14	6.04 ± 0.04	6.02 ± 0.05	6.01 ± 0.04
	50	6.57 ± 0.72	6.11 ± 0.09	6.14 ± 0.21	6.13 ± 0.12	6.17 ± 0.2	6.01 ± 0.04	6.01 ± 0.04	6.0 ± 0.04
	100	6.4 ± 0.62	6.07 ± 0.12	6.25 ± 0.33	6.2 ± 0.41	6.24 ± 0.34	6.01 ± 0.04	6.01 ± 0.04	6.0 ± 0.04
<i>Pendulum</i>	10	0.28 ± 0.06	0.39 ± 0.24	0.64 ± 0.48	0.34 ± 0.19	0.34 ± 0.25	0.12 ± 0.04	0.15 ± 0.06	0.17 ± 0.08
	25	0.22 ± 0.08	0.23 ± 0.3	0.15 ± 0.12	0.12 ± 0.09	0.11 ± 0.07	0.09 ± 0.03	0.09 ± 0.03	0.09 ± 0.02
	50	0.18 ± 0.08	0.13 ± 0.1	0.14 ± 0.14	0.15 ± 0.12	0.11 ± 0.1	0.06 ± 0.03	0.06 ± 0.05	0.05 ± 0.01
	100	0.15 ± 0.04	0.06 ± 0.03	0.07 ± 0.04	0.08 ± 0.05	0.05 ± 0.03	0.06 ± 0.01	0.05 ± 0.04	0.05 ± 0.01
<i>Hopper</i>	10	1.6 ± 0.19	1.03 ± 0.29	1.23 ± 0.44	1.05 ± 0.38	1.06 ± 0.32	0.55 ± 0.09	0.66 ± 0.08	0.69 ± 0.1
	25	1.24 ± 0.26	0.64 ± 0.16	0.7 ± 0.21	0.63 ± 0.2	0.61 ± 0.12	0.36 ± 0.06	0.38 ± 0.05	0.39 ± 0.06
	50	1.14 ± 0.16	0.53 ± 0.13	0.5 ± 0.1	0.53 ± 0.16	0.61 ± 0.26	0.31 ± 0.04	0.33 ± 0.03	0.34 ± 0.04
	100	0.97 ± 0.2	0.62 ± 0.18	0.62 ± 0.21	0.68 ± 0.23	0.64 ± 0.2	0.32 ± 0.02	0.3 ± 0.03	0.29 ± 0.03
<i>Ant</i>	10	1.33 ± 0.1	2.23 ± 0.27	2.14 ± 0.29	2.21 ± 0.33	2.03 ± 0.22	1.24 ± 0.13	1.25 ± 0.07	1.29 ± 0.07
	25	1.13 ± 0.09	2.21 ± 0.31	2.2 ± 0.32	2.13 ± 0.24	2.05 ± 0.19	1.13 ± 0.1	1.16 ± 0.07	1.2 ± 0.09
	50	1.05 ± 0.05	2.21 ± 0.24	2.09 ± 0.42	1.93 ± 0.2	2.22 ± 0.58	1.05 ± 0.03	1.09 ± 0.04	1.1 ± 0.04
	100	1.05 ± 0.1	1.93 ± 0.3	2.11 ± 0.26	1.91 ± 0.22	1.84 ± 0.17	1.01 ± 0.05	1.06 ± 0.08	1.1 ± 0.07
<i>Humanoid</i>	10	8.79 ± 1.17	11.51 ± 0.45	11.17 ± 0.2	10.97 ± 0.15	11.07 ± 0.26	10.69 ± 1.05	6.82 ± 1.34	7.5 ± 1.63
	25	6.97 ± 1.48	11.4 ± 0.24	11.22 ± 0.37	11.01 ± 0.17	11.16 ± 0.2	10.65 ± 0.81	5.11 ± 1.34	5.3 ± 1.51
	50	7.0 ± 1.34	11.3 ± 0.24	11.21 ± 0.31	11.07 ± 0.25	11.28 ± 0.19	10.94 ± 0.58	4.27 ± 0.94	4.08 ± 0.8
	100	6.59 ± 1.54	11.28 ± 0.16	10.99 ± 0.33	11.01 ± 0.23	11.35 ± 0.16	10.71 ± 0.43	3.4 ± 0.48	3.37 ± 0.44

 $p < 0.05$
 $p < 0.01$
 $p < 0.001$

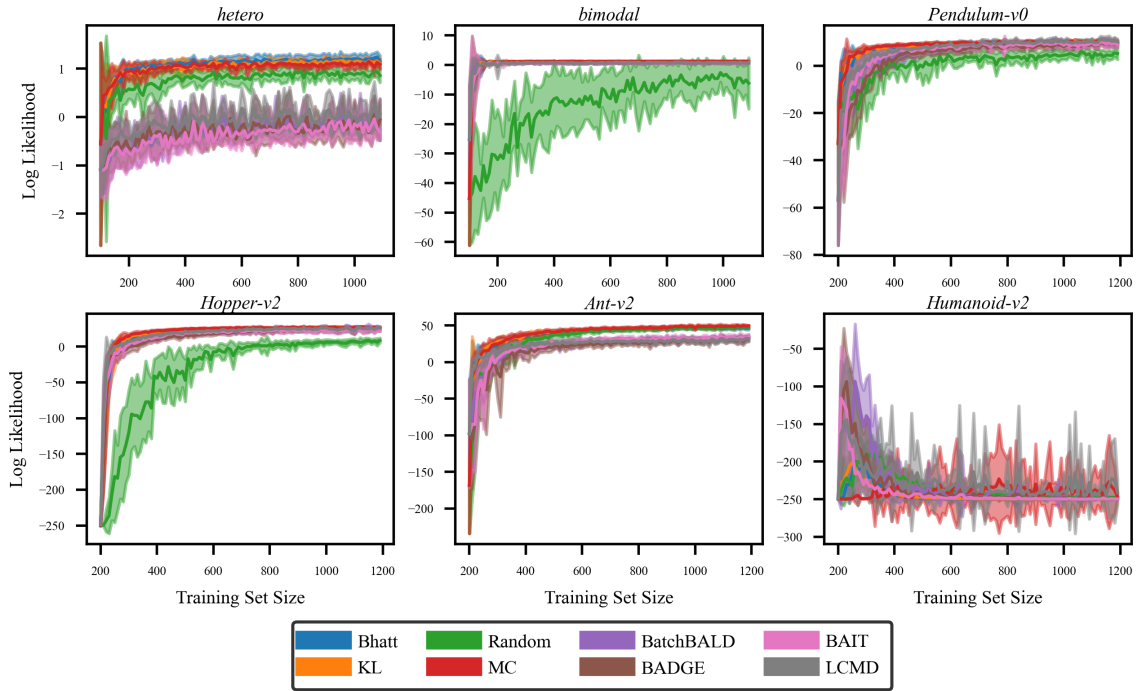


Figure 8: Mean Log Likelihood on test set as data was added to the training sets for Nflows Base.

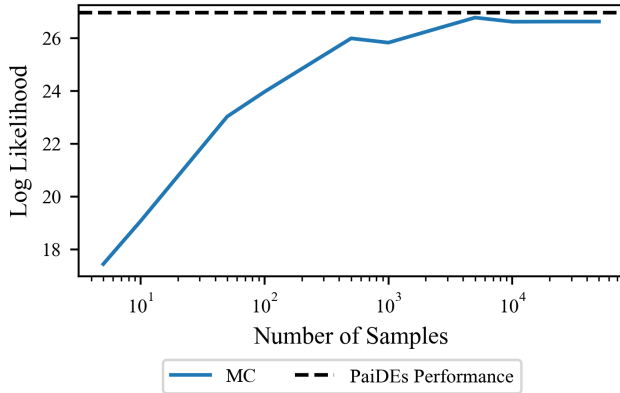


Figure 9: Log-Likelihood on the test set at the 100th acquisition batch of the MC estimator on the *Hopper* environment as the number of samples increases, K , for Nflows Base. Experiment run across 10 seeds and the mean is being reported.

Efficient Epistemic Uncertainty Estimation

Table 3: Log Likelihood of a held out test set during training at different acquisition batches for Nflows Base. Experiments were across ten different seeds and the results are expressed as mean plus minus one standard deviation.

Env	Acq. Batch	Random	BatchBALD	BADGE	BAIT	LCMD	Monte Carlo	KL	Bhatt
<i>hetero</i>	10	0.54 ± 0.27	-0.59 ± 0.55	-0.49 ± 0.61	-0.65 ± 0.54	-0.43 ± 0.26	0.95 ± 0.12	0.93 ± 0.14	0.99 ± 0.12
	25	0.79 ± 0.18	-0.57 ± 0.35	-0.53 ± 0.24	-0.64 ± 0.31	-0.32 ± 0.21	1.06 ± 0.06	1.06 ± 0.12	1.11 ± 0.09
	50	0.8 ± 0.18	-0.25 ± 0.2	-0.29 ± 0.22	-0.36 ± 0.16	-0.1 ± 0.27	1.08 ± 0.04	1.07 ± 0.16	1.15 ± 0.14
	100	0.86 ± 0.14	-0.05 ± 0.44	-0.06 ± 0.42	-0.31 ± 0.15	0.06 ± 0.21	1.09 ± 0.1	1.12 ± 0.1	1.14 ± 0.13
<i>bimodal</i>	10	-30.57 ± 12.61	0.68 ± 0.29	0.7 ± 0.48	0.75 ± 0.22	0.74 ± 0.39	1.08 ± 0.09	1.11 ± 0.1	1.11 ± 0.1
	25	-16.55 ± 9.04	0.74 ± 0.26	0.8 ± 0.23	0.67 ± 0.32	0.81 ± 0.13	1.21 ± 0.09	1.17 ± 0.1	1.27 ± 0.09
	50	-10.85 ± 8.5	0.67 ± 0.28	0.84 ± 0.22	0.82 ± 0.24	0.74 ± 0.17	1.22 ± 0.11	1.2 ± 0.1	1.21 ± 0.11
	100	-6.19 ± 8.66	0.84 ± 0.25	0.83 ± 0.25	0.92 ± 0.33	0.89 ± 0.27	1.26 ± 0.13	1.26 ± 0.1	1.26 ± 0.14
<i>Pendulum</i>	10	-5.55 ± 6.8	-0.99 ± 2.71	-8.64 ± 4.52	-0.2 ± 3.58	0.12 ± 3.42	5.81 ± 3.29	6.17 ± 1.86	5.8 ± 1.41
	25	-0.78 ± 5.92	5.25 ± 2.42	5.52 ± 1.81	6.94 ± 1.58	7.09 ± 1.69	8.72 ± 0.45	8.45 ± 0.55	8.3 ± 0.7
	50	3.77 ± 1.8	8.41 ± 1.55	7.8 ± 1.71	8.24 ± 2.06	8.38 ± 1.51	9.77 ± 0.36	9.95 ± 0.5	9.59 ± 0.27
	100	5.19 ± 2.45	9.46 ± 1.03	8.94 ± 1.15	8.9 ± 1.36	10.22 ± 1.14	10.16 ± 0.7	10.49 ± 0.23	9.58 ± 0.8
<i>Hopper</i>	10	-136.85 ± 53.59	1.49 ± 6.05	-3.93 ± 6.13	0.33 ± 6.2	4.69 ± 2.87	13.94 ± 5.54	11.59 ± 4.32	11.44 ± 2.31
	25	-28.0 ± 28.16	15.86 ± 2.43	13.64 ± 2.93	17.54 ± 2.08	18.53 ± 2.05	23.18 ± 1.41	22.71 ± 0.86	22.29 ± 0.95
	50	-0.55 ± 6.82	22.46 ± 2.42	21.98 ± 3.26	23.06 ± 3.95	23.66 ± 3.18	26.43 ± 1.37	25.72 ± 1.04	25.0 ± 1.6
	100	8.67 ± 3.39	25.9 ± 1.89	24.4 ± 2.98	23.82 ± 2.39	26.07 ± 1.64	26.62 ± 1.14	26.96 ± 1.11	26.88 ± 0.91
<i>Ant</i>	10	-0.5 ± 16.68	1.09 ± 12.41	-2.24 ± 12.36	-1.35 ± 13.33	17.54 ± 6.36	24.48 ± 5.88	25.41 ± 5.08	21.59 ± 9.0
	25	31.08 ± 5.4	22.52 ± 4.73	16.87 ± 7.39	22.0 ± 4.7	23.35 ± 4.48	39.77 ± 3.34	40.62 ± 2.85	37.58 ± 2.37
	50	43.37 ± 1.85	28.03 ± 3.53	26.73 ± 3.35	30.84 ± 2.19	28.92 ± 2.59	45.67 ± 1.76	45.07 ± 1.62	44.77 ± 1.39
	100	47.52 ± 1.36	33.69 ± 3.1	31.57 ± 3.42	35.39 ± 2.6	31.89 ± 3.94	49.29 ± 0.78	48.12 ± 2.05	46.52 ± 2.42
<i>Humanoid</i>	10	-200.61 ± 20.02	-153.76 ± 48.74	-200.56 ± 37.2	-230.61 ± 9.92	-220.73 ± 20.19	-249.1 ± 0.69	-221.09 ± 10.68	-201.28 ± 22.78
	25	-223.54 ± 13.72	-231.51 ± 16.72	-238.87 ± 14.85	-245.86 ± 1.8	-226.07 ± 26.57	-247.84 ± 1.74	-246.29 ± 1.92	-247.16 ± 1.04
	50	-244.15 ± 1.52	-247.03 ± 2.56	-246.62 ± 4.16	-248.41 ± 0.93	-235.55 ± 13.35	-247.76 ± 2.11	-249.39 ± 0.43	-249.57 ± 0.62
	100	-247.82 ± 1.28	-249.38 ± 0.69	-249.15 ± 0.69	-249.71 ± 0.32	-241.1 ± 16.55	-246.47 ± 2.99	-249.76 ± 0.4	-249.97 ± 0.05

■ $p < 0.05$
■ $p < 0.01$
■ $p < 0.001$

E. Probabilistic Network Ensembles

In addition to ensembles of normalizing flows, we also explored the use of probabilistic network ensembles (PNEs) as a common approach for capturing uncertainty (Chua et al., 2018; Kurutach et al., 2018; Lakshminarayanan et al., 2017). The PNEs were constructed by employing fixed dropout masks, where each ensemble component modeled a Gaussian distribution. The models were trained using negative log likelihood, with weights randomly initialized and bootstrapped samples from the training set to create diversity amongst the components. Our findings paralleled those of Nflows Base, in that PaiDEs performed similarly or better than baselines and statistically significantly in higher dimensions. These results are presented in s Figure 11 and Figure 12, as well as Table 4 and Table 5. Note that PNEs did not perform as well as Nflows Base as they are not as expressive this can be seen for the *bimodal* setting in Figure 10. Furthermore, we have included the 1D graphs illustrating the performance of PNEs in *hetero* and *bimodal* in Figure 10. Similarly to before, we also provide a comparison of the MC estimator as the number of samples increased in Figure 13. While we could have implemented ensembles with different output distributions to better fit the data, we decided to stick with Gaussians as they seem to be the most frequent choice (Chua et al., 2018; Kurutach et al., 2018; Lakshminarayanan et al., 2017). Moreover, in order to pick the best distributional fit would require a hyper-parameter search or apriori knowledge whereas NFs will learn the best distributional fit.

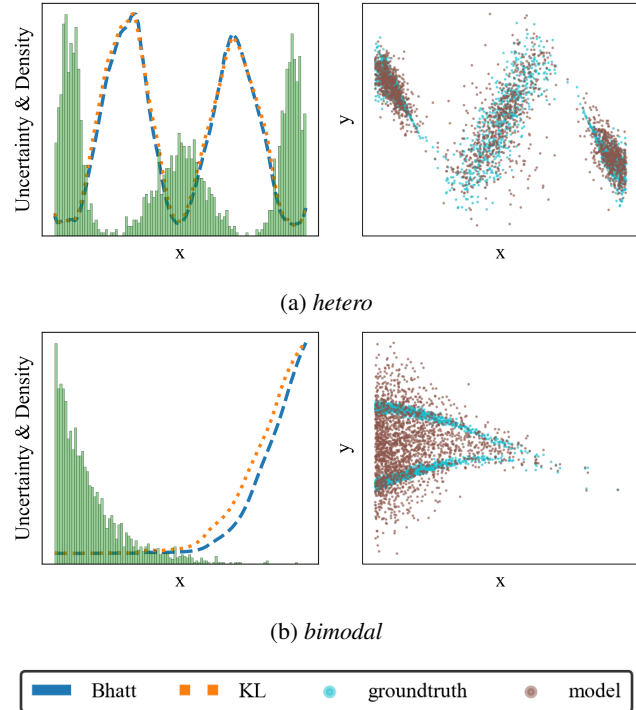


Figure 10: In the right graphs, the cyan dots are the ground-truth data and the brown dots are sampled from PNEs. The 2 lines depict epistemic uncertainty corresponding to different estimators. The left graphs depicts the ground-truth data as the blue dots and its corresponding density as the orange histogram. Note the legend refers to the lines in the right graphs.

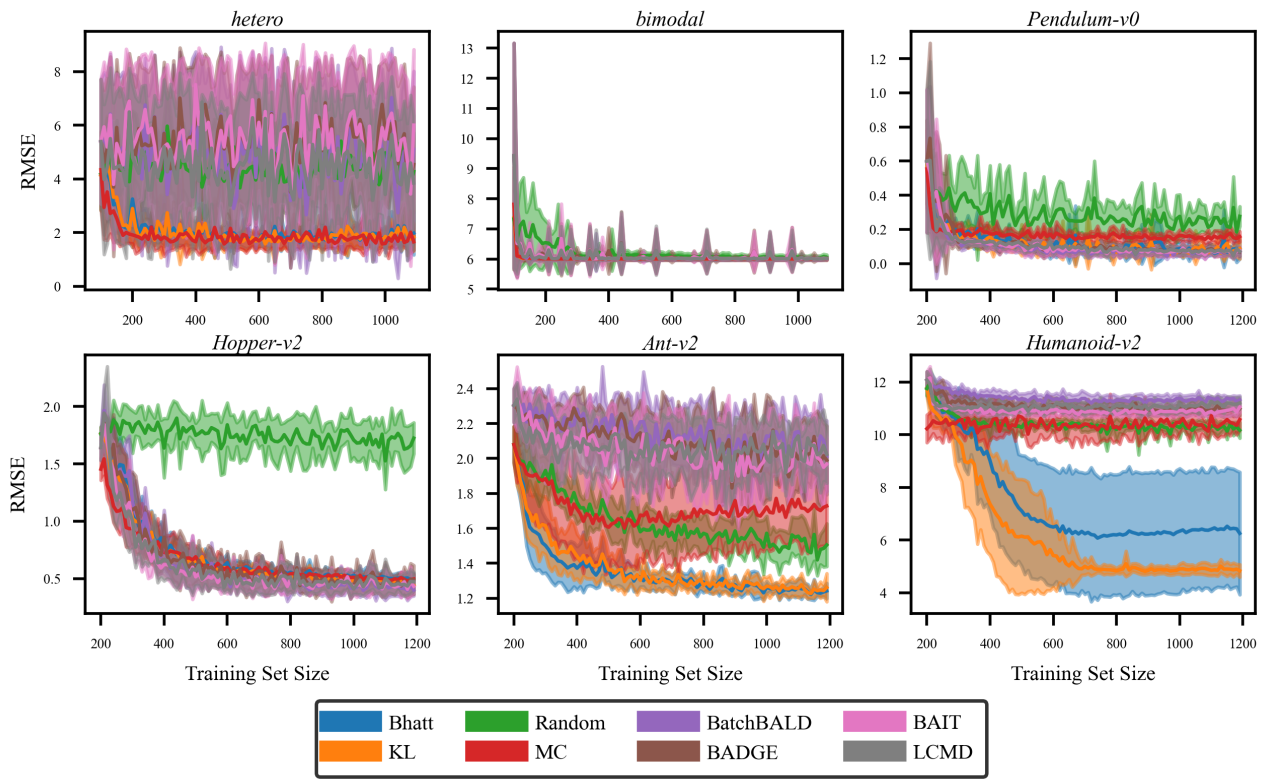


Figure 11: Mean RMSE on test set as data was added to the training sets for PNEs.

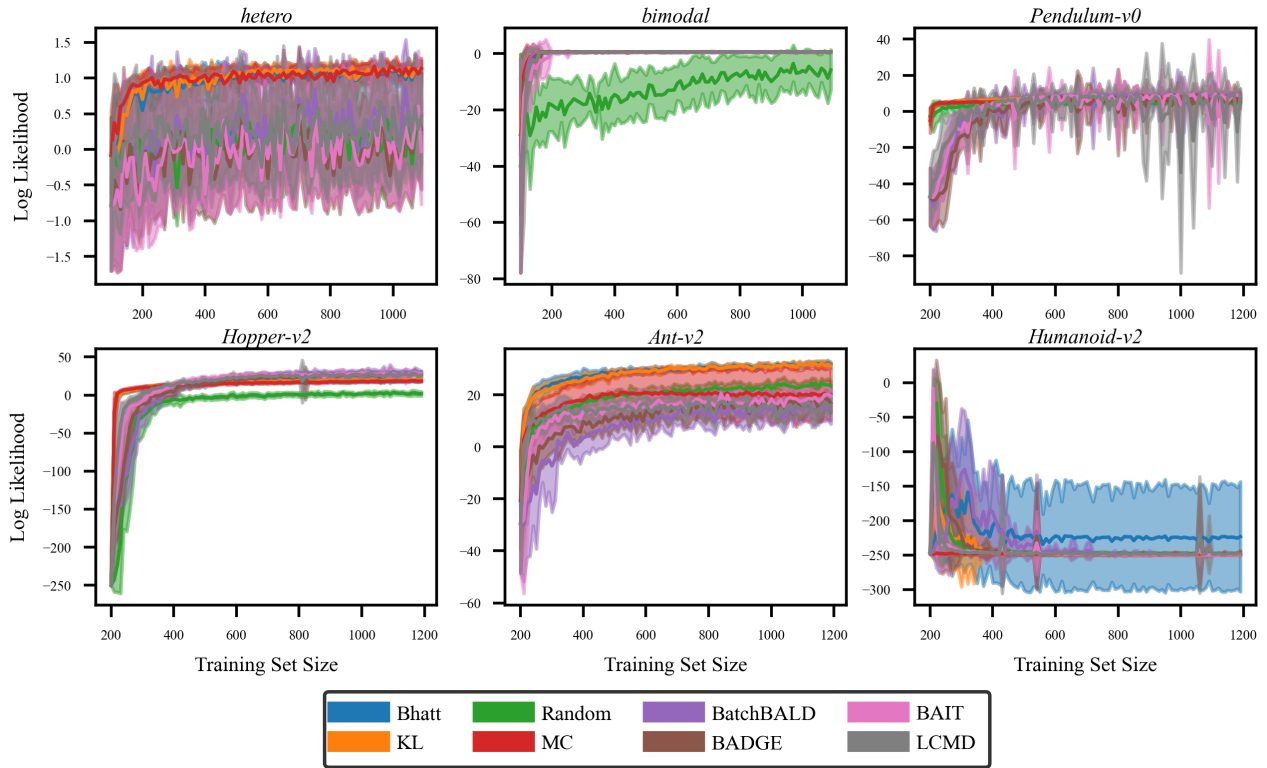


Figure 12: Mean Log Likelihood on the test set as data was added to the training sets for PNEs.

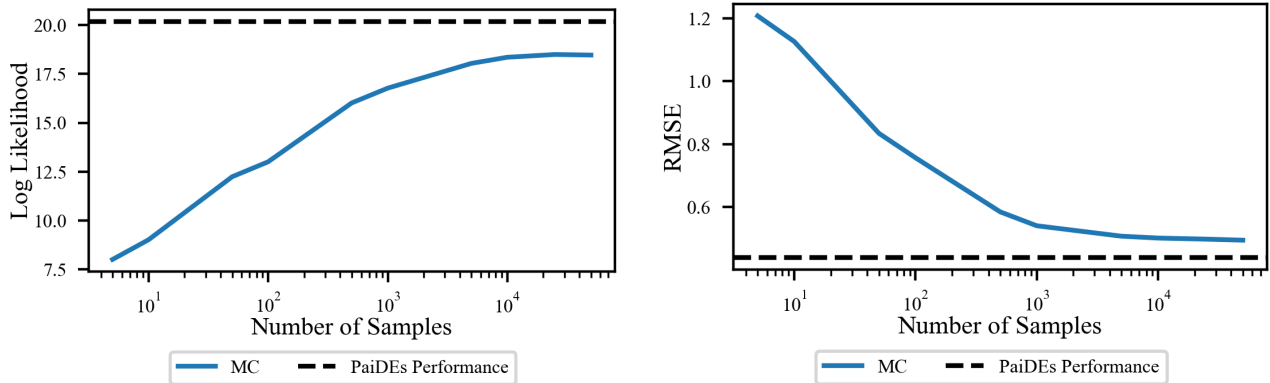


Figure 13: RMSE and Log-Likelihood on the test set at the 100^{th} acquisition batch of the MC estimator on the *Hopper* environment as the number of samples increases, K , for PNEs. Experiment run across 10 seeds and the mean is being reported.

Table 4: Mean RMSE on the test set for certain Acquisition Batches for PNEs. Experiments were across ten different seeds and the results are expressed as mean plus minus one standard deviation. Note that nothing was bolded for *bimodal* as many methods performed similarly.

Env	Acq. Batch	Random	BatchBALD	BADGE	BAIT	LCMD	Monte Carlo	KL	Bhatt
<i>hetero</i>	10	3.9 ± 1.47	6.9 ± 1.15	6.91 ± 1.77	6.9 ± 1.58	6.49 ± 1.63	1.94 ± 0.34	2.11 ± 0.34	2.36 ± 0.75
	25	4.42 ± 1.43	4.43 ± 2.81	4.06 ± 2.58	5.02 ± 2.91	3.85 ± 2.51	1.75 ± 0.27	1.86 ± 0.39	1.96 ± 0.44
	50	3.96 ± 1.71	4.06 ± 2.64	5.12 ± 2.78	5.22 ± 2.93	4.87 ± 2.36	1.78 ± 0.51	1.68 ± 0.34	1.67 ± 0.27
	100	4.28 ± 1.45	5.1 ± 2.92	4.54 ± 2.89	6.01 ± 2.82	3.85 ± 2.5	1.66 ± 0.31	1.83 ± 0.51	1.98 ± 0.81
<i>bimodal</i>	10	6.52 ± 0.88	6.05 ± 0.07	6.19 ± 0.27	6.11 ± 0.15	6.05 ± 0.06	6.01 ± 0.04	6.02 ± 0.04	6.01 ± 0.04
	25	6.1 ± 0.08	6.26 ± 0.75	6.31 ± 0.83	6.3 ± 0.88	6.28 ± 0.8	6.01 ± 0.04	6.01 ± 0.04	6.01 ± 0.04
	50	6.13 ± 0.13	6.01 ± 0.04	6.04 ± 0.07	6.02 ± 0.03	6.01 ± 0.04	6.01 ± 0.04	6.01 ± 0.04	6.01 ± 0.04
	100	6.06 ± 0.08	6.01 ± 0.03	6.03 ± 0.03	6.01 ± 0.04	6.01 ± 0.03	6.01 ± 0.04	6.01 ± 0.04	6.01 ± 0.04
<i>Pendulum</i>	10	0.31 ± 0.11	0.15 ± 0.02	0.16 ± 0.05	0.15 ± 0.03	0.16 ± 0.03	0.19 ± 0.04	0.18 ± 0.06	0.2 ± 0.07
	25	0.27 ± 0.09	0.11 ± 0.03	0.12 ± 0.03	0.11 ± 0.03	0.12 ± 0.03	0.16 ± 0.02	0.12 ± 0.04	0.13 ± 0.04
	50	0.25 ± 0.07	0.08 ± 0.02	0.09 ± 0.02	0.08 ± 0.02	0.09 ± 0.03	0.15 ± 0.03	0.08 ± 0.02	0.09 ± 0.03
	100	0.28 ± 0.06	0.07 ± 0.03	0.07 ± 0.02	0.08 ± 0.02	0.07 ± 0.02	0.16 ± 0.03	0.09 ± 0.06	0.08 ± 0.05
<i>Hopper</i>	10	1.85 ± 0.14	1.44 ± 0.31	1.12 ± 0.29	1.16 ± 0.37	1.09 ± 0.36	0.94 ± 0.16	1.19 ± 0.21	1.14 ± 0.18
	25	1.9 ± 0.14	0.6 ± 0.13	0.66 ± 0.19	0.55 ± 0.12	0.54 ± 0.14	0.73 ± 0.13	0.72 ± 0.08	0.71 ± 0.1
	50	1.83 ± 0.13	0.54 ± 0.15	0.55 ± 0.15	0.51 ± 0.12	0.51 ± 0.12	0.57 ± 0.06	0.57 ± 0.06	0.57 ± 0.05
	100	1.72 ± 0.14	0.4 ± 0.05	0.49 ± 0.13	0.43 ± 0.05	0.47 ± 0.08	0.5 ± 0.04	0.44 ± 0.04	0.49 ± 0.05
<i>Ant</i>	10	1.89 ± 0.12	2.27 ± 0.13	2.24 ± 0.12	2.15 ± 0.18	2.09 ± 0.19	1.87 ± 0.25	1.62 ± 0.16	1.52 ± 0.18
	25	1.74 ± 0.13	2.15 ± 0.21	2.14 ± 0.18	2.12 ± 0.25	2.08 ± 0.13	1.67 ± 0.25	1.43 ± 0.12	1.39 ± 0.12
	50	1.55 ± 0.1	2.2 ± 0.13	2.16 ± 0.14	2.11 ± 0.18	2.07 ± 0.16	1.61 ± 0.22	1.29 ± 0.06	1.3 ± 0.04
	100	1.5 ± 0.12	2.01 ± 0.2	1.99 ± 0.2	1.97 ± 0.15	2.02 ± 0.16	1.73 ± 0.22	1.26 ± 0.08	1.24 ± 0.04
<i>Humanoid</i>	10	10.73 ± 0.32	11.63 ± 0.19	11.22 ± 0.29	10.95 ± 0.17	10.98 ± 0.16	10.41 ± 0.53	9.95 ± 1.1	10.65 ± 0.84
	25	10.38 ± 0.22	11.36 ± 0.26	11.07 ± 0.26	10.91 ± 0.25	11.06 ± 0.23	10.44 ± 0.55	6.54 ± 2.13	8.22 ± 2.47
	50	10.29 ± 0.19	11.37 ± 0.3	10.98 ± 0.22	10.9 ± 0.25	11.01 ± 0.22	10.34 ± 0.81	4.91 ± 0.24	6.33 ± 2.24
	100	10.17 ± 0.3	11.32 ± 0.16	10.99 ± 0.26	11.05 ± 0.21	11.2 ± 0.23	10.57 ± 0.41	4.84 ± 0.24	6.25 ± 2.32

 $p < 0.05$
 $p < 0.01$
 $p < 0.001$

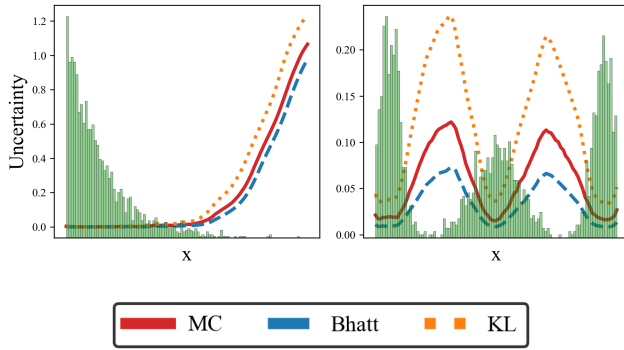


Figure 14: The same plots as Figure 2 except there is no mapping applied and the corresponding estimates for $I(y, W)$ are shown the right y-axes for the right plots.

Efficient Epistemic Uncertainty Estimation

Table 5: Log Likelihood on the test set during training at different acquisition batches for PNEs. Experiments were across ten different seeds and the results are expressed as mean plus minus one standard deviation. Note that no values were highlighted for Hopper despite the results being statistically significant. In this case, the results are statistically significantly worse and we found it misleading to highlight.

Env	Acq. Batch	Random	BatchBALD	BADGE	BAIT	LCMD	Monte Carlo	KL	Bhatt
<i>hetero</i>	10	0.13 ± 0.57	-0.67 ± 0.55	-0.72 ± 0.61	-0.78 ± 0.59	-0.46 ± 0.49	0.89 ± 0.1	0.87 ± 0.15	0.74 ± 0.3
	25	0.03 ± 0.47	0.33 ± 0.76	0.38 ± 0.76	0.13 ± 0.82	0.41 ± 0.75	1.02 ± 0.11	0.95 ± 0.14	0.92 ± 0.24
	50	0.23 ± 0.57	0.48 ± 0.71	0.14 ± 0.77	0.11 ± 0.85	0.17 ± 0.69	1.01 ± 0.15	1.1 ± 0.11	1.09 ± 0.12
	100	0.23 ± 0.42	0.23 ± 0.78	0.28 ± 0.85	-0.03 ± 0.74	0.46 ± 0.7	1.1 ± 0.11	1.11 ± 0.17	1.08 ± 0.2
<i>bimodal</i>	10	-17.71 ± 10.01	0.32 ± 0.33	0.41 ± 0.21	-1.36 ± 4.14	0.2 ± 0.49	0.6 ± 0.1	0.59 ± 0.14	0.61 ± 0.07
	25	-20.78 ± 5.64	0.61 ± 0.19	0.48 ± 0.23	0.57 ± 0.21	0.57 ± 0.21	0.66 ± 0.03	0.66 ± 0.03	0.67 ± 0.04
	50	-12.93 ± 8.55	0.66 ± 0.09	0.59 ± 0.16	0.61 ± 0.18	0.67 ± 0.09	0.69 ± 0.02	0.69 ± 0.03	0.69 ± 0.03
	100	-5.79 ± 7.19	0.66 ± 0.1	0.64 ± 0.11	0.68 ± 0.08	0.67 ± 0.1	0.7 ± 0.02	0.7 ± 0.02	0.7 ± 0.02
<i>Pendulum</i>	10	2.35 ± 2.94	-10.76 ± 7.28	-15.25 ± 8.86	-9.76 ± 9.09	-3.4 ± 2.6	4.94 ± 0.48	5.51 ± 0.72	5.21 ± 0.61
	25	4.19 ± 0.89	-0.4 ± 14.08	0.2 ± 13.03	4.68 ± 2.98	5.42 ± 5.25	5.45 ± 0.43	6.21 ± 0.98	6.23 ± 0.84
	50	4.34 ± 0.75	8.34 ± 0.83	7.97 ± 0.74	8.68 ± 0.72	8.13 ± 0.94	5.92 ± 0.32	7.65 ± 0.5	7.15 ± 0.76
	100	4.69 ± 0.56	9.53 ± 0.96	7.07 ± 5.49	8.8 ± 1.23	9.27 ± 0.83	6.09 ± 0.42	7.66 ± 0.64	7.77 ± 0.68
<i>Hopper</i>	10	-31.94 ± 28.24	-26.65 ± 15.57	-12.96 ± 9.55	-10.81 ± 4.25	-2.04 ± 5.45	9.36 ± 1.79	8.55 ± 1.34	8.55 ± 1.88
	25	-5.74 ± 2.66	12.62 ± 4.32	13.88 ± 2.27	17.29 ± 3.45	16.69 ± 1.7	13.31 ± 2.3	13.9 ± 1.3	13.93 ± 1.6
	50	-2.31 ± 3.08	27.28 ± 2.42	23.49 ± 2.97	28.08 ± 2.76	24.73 ± 1.71	16.43 ± 1.27	17.6 ± 1.89	16.93 ± 1.43
	100	1.75 ± 2.83	30.35 ± 1.44	26.54 ± 2.19	28.44 ± 1.52	26.22 ± 2.75	18.5 ± 0.65	20.19 ± 1.37	18.54 ± 1.23
<i>Ant</i>	10	11.83 ± 2.29	-4.91 ± 12.37	3.29 ± 6.43	10.2 ± 5.57	12.39 ± 3.69	13.8 ± 5.87	22.13 ± 3.11	23.32 ± 2.73
	25	17.78 ± 2.28	5.79 ± 7.68	8.44 ± 3.68	11.97 ± 5.41	12.37 ± 4.35	18.69 ± 9.06	26.98 ± 1.64	27.66 ± 1.78
	50	22.21 ± 2.11	12.24 ± 3.25	14.94 ± 3.3	16.16 ± 3.2	14.41 ± 3.79	20.54 ± 8.88	29.84 ± 1.09	29.62 ± 0.7
	100	23.4 ± 1.85	15.26 ± 6.5	16.87 ± 3.75	19.6 ± 2.07	16.08 ± 2.67	20.03 ± 9.87	31.24 ± 1.09	31.63 ± 0.9
<i>Humanoid</i>	10	-230.41 ± 19.87	-156.59 ± 82.79	-210.52 ± 53.23	-242.95 ± 2.96	-244.1 ± 3.79	-247.83 ± 1.71	-226.42 ± 46.74	-194.78 ± 73.74
	25	-245.45 ± 2.24	-224.95 ± 37.12	-245.82 ± 5.03	-247.3 ± 1.26	-245.87 ± 4.85	-247.83 ± 1.19	-247.39 ± 3.18	-232.34 ± 42.02
	50	-246.91 ± 1.28	-247.38 ± 3.28	-249.28 ± 0.52	-249.2 ± 0.52	-248.59 ± 1.68	-248.06 ± 1.82	-249.41 ± 0.73	-223.49 ± 77.83
	100	-247.74 ± 0.6	-248.97 ± 1.1	-249.4 ± 0.6	-249.66 ± 0.53	-248.13 ± 1.25	-247.25 ± 3.36	-249.91 ± 0.12	-223.29 ± 79.8

$p < 0.05$
 $p < 0.01$
 $p < 0.001$

F. Introduction to Normalizing Flows

NFs are powerful non-parametric models that have demonstrated the ability to fit flexible multi-modal distributions (Tabak & Vanden-Eijnden, 2010; Tabak & Turner, 2013). These models achieve this by transforming a simple base continuous distribution, such as Gaussian or Beta, into a more complex one using the change of variable formula. By enabling scoring and sampling from the fitted distribution, NFs find application across various problem domains. Let B represent the base distribution, a D -dimensional continuous random vector with $p_B(b)$ as its density function, and let $Y = g(B)$, where g is an invertible function with an existing inverse g^{-1} , and both g and g^{-1} are differentiable. Leveraging the change of variable formula, we can express the distribution of Y as follows:

$$p_Y(y) = p_B(g^{-1}(y)) |\det(J(g^{-1}(y)))|, \quad (12)$$

where $J(\cdot)$ denotes the Jacobian, and \det signifies the determinant. The first term on the right-hand side of Equation 12 governs the shape of the distribution, while $|\det(J(g^{-1}(y)))|$ normalizes it, ensuring the distribution integrates to one. Complex distributions can be effectively modeled by making $g(b)$ a learnable function with tunable parameters θ , denoted as $g_\theta(b)$. However, it is essential to select g carefully to guarantee its invertibility and differentiability. For examples of suitable choices, please refer to (Papamakarios et al., 2021).

G. Hypothesis Testing Details

We conducted Welch’s t-tests to compare means (μ_i, μ_j) between different estimators, as this test relaxes the assumption of equal variances compared to other hypothesis tests (Colas et al., 2019). The means for both KL and Bhatt were compared to each of the baseline methods: BatchBALD, BADGE, BAIT, LCMD, MC and random. To control the family-wise error rate (FWER), we performed a Holm-Bonferroni correction across each setting, environment, and acquisition batch. This follows best practices to ensure our results are statistically significant and do not occur just by random chance.